Qian, Yutong, Jie, Dongmei, Niu, Honghao, Gao, Guizai, Chambers, Frank M ORCID logoORCID: https://orcid.org/0000-0002-0998-2093 and Liu, Ziping (2024) Climate-driven peatlands development and vegetation dynamics in Northeastern China since the mid-Holocene: New evidence from Huanan peatlands. Palaeogeography, Palaeoclimatology, Palaeoecology, 655. art: 112544. doi:10.1016/j.palaeo.2024.112544

Official URL: http://doi.org/10.1016/j.palaeo.2024.112544
DOI: http://dx.doi.org/10.1016/j.palaeo.2024.112544
EPrint URI: https://eprints.glos.ac.uk/id/eprint/14443

Climate-driven peatlands development and vegetation dynamics in Northeastern China since the mid-Holocene: new evidence from Huanan peatlands

Yutong Qian[a], Dongmei Jie[a,b,c,*], Honghao Niu[d,*], Guizai Gao [a,b,c], Frank M. Chambers[e], Ziping Liu[a]

[a]Key Laboratory of Geographical Processes and Ecological Security in Changbai Mountains, Ministry of Education, Changchun 130024, China

[b]Institute for Peat and Mire Research, State Environmental Protection Key Laboratory of Wetland Ecology and Vegetation Restoration, Changchun 130024, China

[c]Institute of Grassland Science, Key Laboratory for Vegetation Ecology, Ministry of Education, Changchun 130024, China

[d]School of Archaeology, Jilin University, Changchun, China

[e]School of Natural and Social Sciences, University of Gloucestershire, Gloucester and Cheltenham, UK

[*]Corresponding authors.

Abstract

Studying peatland evolution and vegetation patterns in response to climate change provides valuable insights into future ecosystem trends. This study focuses on the Huanan peatland located in Changbai Mountain regions in Northeast China, utilizing phytolith analysis and stable carbon isotope composition ($\delta^{13}C$) to reconstruct late Holocene vegetation dynamics. Additionally, grain size, total organic carbon (TOC), and total nitrogen (TN) analyses were conducted to understand peatland development and paleoclimate since the late Holocene. The research identifies three distinct climate periods since 5500 cal yr BP: an initial warm, humid phase (5500-4000 cal yr BP) characterized by high river levels that formed lacustrine sediments; a subsequent transition to cold, dry conditions (4000-1500 cal yr BP) that initiated peat formation; and continued dry, cold conditions (1500 cal yr BP to the present) with sustained peat growth. Phytolith data reveal a dominant forest vegetation type since 2000 cal yr BP, further divided into three periods: 2000-1300 cal yr BP, marked by diverse and dense vegetation; 1300-750 cal yr BP, with declining plant cover; and 750 cal yr

BP to the present, characterized by an increase in woody plants but a reduction in local grass cover.

Keywords

mid-late Holocene, paleovegetation, paleoclimate, peatland development process, peatland

1. Introduction

Peatlands play a crucial role in the global carbon cycle owing to their substantial carbon sequestration capacity (Charman et al., 2015; Loisel et al., 2017; Gallego-Sala et al., 2018; Loisel et al., 2021), storing approximately one-third of the total global soil carbon pool (Yu et al., 2010; Yu et al., 2021). Thus, understanding the long-term evolution process of peatland ecosystems is a current focal point within the academic community and research primarily focuses on two aspects: the development and accumulation of peatland (Mathijssen et al., 2016; Panait et al., 2017) and the evolution of vegetation covering the peatland (Johnson et al., 2005; Lou et al., 2013). Research on peatland evolution in China has primarily concentrated on the Northeastern region (Cai et al., 2013; Sun et al., 2019; Zhang et al., 2021), the Qinghai-Tibet Plateau (Zhao et al., 2014; Wang et al., 2014; Sun et al., 2017), and the Altai Mountains of Xinjiang (Zhang et al., 2020). Northeast China is recognized as the largest peat swamp distribution area in China (Niu et al., 2012; Xing et al., 2015). Despite this focus, the influencing factors of peatland development and evolution in Northeast China have not been thoroughly explored. Previous studies have predominantly emphasized regional climate conditions as the primary factor (Wang et al., 2014; Charman et al., 2015; Zhang et al., 2015), with less attention given to local conditions. Nevertheless, local conditions play a crucial role in peatland evolution (van Bellen et al., 2011; Lacourse and Davies, 2015; Panait et al., 2017; Mathijssen et al., 2019), but the specific mechanism remains unclear. Furthermore, existing research lacks a comprehensive analysis that integrates regional and local scale factors to investigate peatland evolution.

The Changbai Mountains in Northeast China are located in the southern part of the global northern peatland distribution belt, making this region a significant area for peatland distribution within the country (Niu et al., 2012; Xing et al., 2015). The peatlands in this area exhibit wide distribution, diverse variety, and long-term development and they are particularly susceptible to the effects of climate change (Zhao et al., 2023). Owing to the predominant presence of nature reserves in the Changbai Mountain peatland, human disturbances are minimal, resulting in relatively continuous and complete peatland deposition. This makes it an ideal location for researching the evolution of peatland ecosystems (Zhang et al., 2020). However, existing research primarily focuses on the Longgang volcanic regions of Changbai Mountain, such as Hani (Cai et al., 2013; Zhang et al., 2021), Jinchuan (Sun et al., 2019; Zhang et al., 2019), Gushantun (Zhang et al., 2020), and Baijianghe (Xia et al., 2019; Dong et al., 2023). There is a noticeable lack of research on the evolution of peatlands in the high-latitude regions of the northern Changbai Mountains, leading to an incomplete understanding of the historical development of peatlands in the Changbai Mountains (cf. Charman, 2002).

The Huanan peatland, located in the lower-altitude mountain valleys of the northern Changbai Mountains, presents an excellent opportunity for study. Investigating the development and evolutionary processes of the Huanan peatland can undoubtedly enhance understanding of the typical characteristics of peat development and carbon accumulation in the Changbai Mountains. The evolution of the Huanan peatland remains poorly understood, with preliminary research primarily focusing on low-resolution pollen records that only reconstruct woody-type plants around the peatland (Jie et al., 2012). These studies lack an emphasis on the quantitative characteristics of vegetation and neglect the reconstruction of local herbaceous and understory herbs (Strömberg, 2004; Strömberg et al., 2007; Fyfe et al., 2013; Mazier et al., 2015). Therefore, it is imperative to incorporate phytolith analysis methods to achieve a more precise identification of herbaceous plants in paleovegetation reconstruction, addressing the limitations inherent in pollen analysis.

Phytoliths are hydrated silicon formed in the gaps between plant cells (Piperno, 2006). Upon the decomposition of the parent plant, they are released directly into the soil, making them ideal for in situ sedimentation and providing valuable insights into local vegetation (Strömberg et al., 2007; Gao et al., 2021). In recent years, phytoliths have become a common tool in research on reconstructing paleovegetation. They can accurately indicate shifts in plant composition and the relative proportions of herbaceous plants using phytolith indexes and assemblages (Alexandre et al., 1997; Blinnikov et al., 2002; Barboni et al., 2010; Gao et al., 2021). Additionally, changes in forest vegetation coverage can also be reconstructed by analyzing the phytolith index (Alexandre et al., 1997). In recent years, by establishing the relationship between topsoil phytolith assemblages and their corresponding plant communities, it has become possible to reconstruct plant community coverage and species diversity quantitatively (Gao et al., 2021; Yang et al., 2023). Phytolith analysis of the Huanan peatland can compensate for the limitations of pollen analysis and provide a deeper understanding of the quantitative characteristics of the ancient vegetation in Huanan peatlands.

This study focuses on Huanan peatland profiles in the Changbai Mountains, utilizing phytolith analysis and carbon isotope analysis to reconstruct community numerical characteristics quantitatively during the late Holocene. The research also investigates the development and evolution of Huanan peatland by examining grain size, organic carbon, and organic nitrogen content. By analyzing peatland grain size composition, the study reconstructs paleoclimate of the Huanan peatlands since the late Holocene. Furthermore, by integrating regional paleoclimate records, we focus on exploring the response pattern of vegetation community numerical characteristics to climate changes. This study seeks to address the following specific questions: 1. What are the developmental processes and evolution of Huanan peatlands? 2. How do the vegetation community numerical characteristics in Huanan peatland vary? 3. What is the vegetation response pattern of Huanan peatland to climate change?

2. Regional setting

The Changbai Mountains (126°29′39.8″E-130°51′47.7″E, 42°13′20.5″N-46°25′45.2″N) are located on the eastern area of the Eurasian continent and experience a typical temperate continental monsoon climate zone in East Asia. The region has an average annual temperature ranging from 2-6°C, with annual precipitation levels between 600-1000 mm (Li et al., 2001). The primary soil type in the Changbai Mountain is dark brown soil, with albic soil and peat bog soil present. The area is characterized by diverse vegetation types, including temperate coniferous woodland dominated by *Pinus koraiensis*, *Abies*, and *Larix*, etc. and broadleaf trees dominated by *Betula costata*, *Quercus mongolica*, *Ulmus propinqua*, *Juglans mandshurica*, *Tilia spp.*, *Fraxinus mandshurica*, *Acer mono*, etc. (Zhao et al., 2023).

The Huanan Peatland (130°51′40.8″E, 46°25′26.0″N) is situated in Huanan County, Heilongjiang Province, within the middle and low mountainous regions of the Laoyeling Mountains of Wanda Mountains, at an altitude of 208 meters (Fig. 1). This area falls under the cold temperate continental climate zone, characterized by a monsoon climate. Based on long-term meteorological data from the Jiamusi City meteorological station near the peat swamp, the average annual temperature of the peatland is approximately 4°C, with an average annual precipitation of around 705 mm. The primary sources of water for the peatland include atmospheric precipitation, surface runoff, and rivers. The Huanan peatland is located in a mountain valley with a low-lying terrain. The peatland developed on the concave banks of the Xiaobahu River, which flows through the peatland and finally merges into the Woken River. The predominant vegetation cover includes *Artemisia*, along with Cyperaceae, Asteraceae, Polygonaceae, and other plant species.

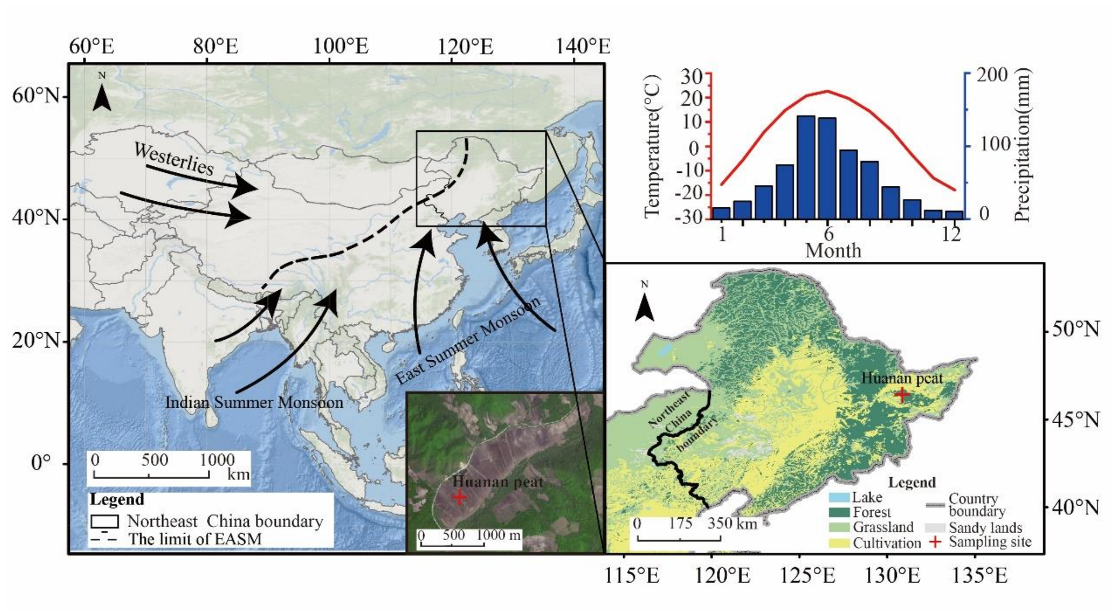

Fig. 1. A. Range of the modern East Asia summer monsoon; B. Satellite image of the Huanan peatland; C. Mean monthly precipitation and temperature for the Huanan peatland; D. The location of the Huanan peatland.

3. Materials and methods

3.1 Sample collection

We collected a 120 cm core of the Huanan peatland in November 2020 (130°51′40.8″E, 46°25′26.0″N) (Fig. 2). According to the lithological characteristics of the section, the core can be divided into 5 layers, from top to bottom: surface layer (0-30 cm), containing a large number of plant roots; gray-brown peat layer (30-60 cm), containing a large number of plant residues; gray-black peat layer, (65-85 cm), with reduced plant residues; black peat layer (85-110 cm); blue gray silt layer (100-120cm). The obtained 120 cm section was sampled at 1 cm intervals in the laboratory, and then stored in a refrigerator. Since the surface layer is affected by human activities, samples from this layer were not analyzed in this study.

3.2 Experimental methods

3.2.1 Radiocarbon dating

To establish the chronology of the Huanan peatland, this study selected four samples from different depths of the Huanan peatland for AMS^{14}C dating (Table 1). The pretreatment process for ^{14}C dating samples involved the internationally recognized method to remove calcium carbonate (Piotrowska et al., 2011). Sample pretreatment was conducted at Northeast Normal University, while sample testing was carried out at the Guangzhou Institute of Geochemistry, Chinese Academy of Science. The obtained age data were calibrated to calendar age using the InCal21 curve (Kennett et al., 2011), and then the Bacon v2.2 model was used to establish the age sequence of the entire section by simulating the relationship between depth and age (Fig. 2).

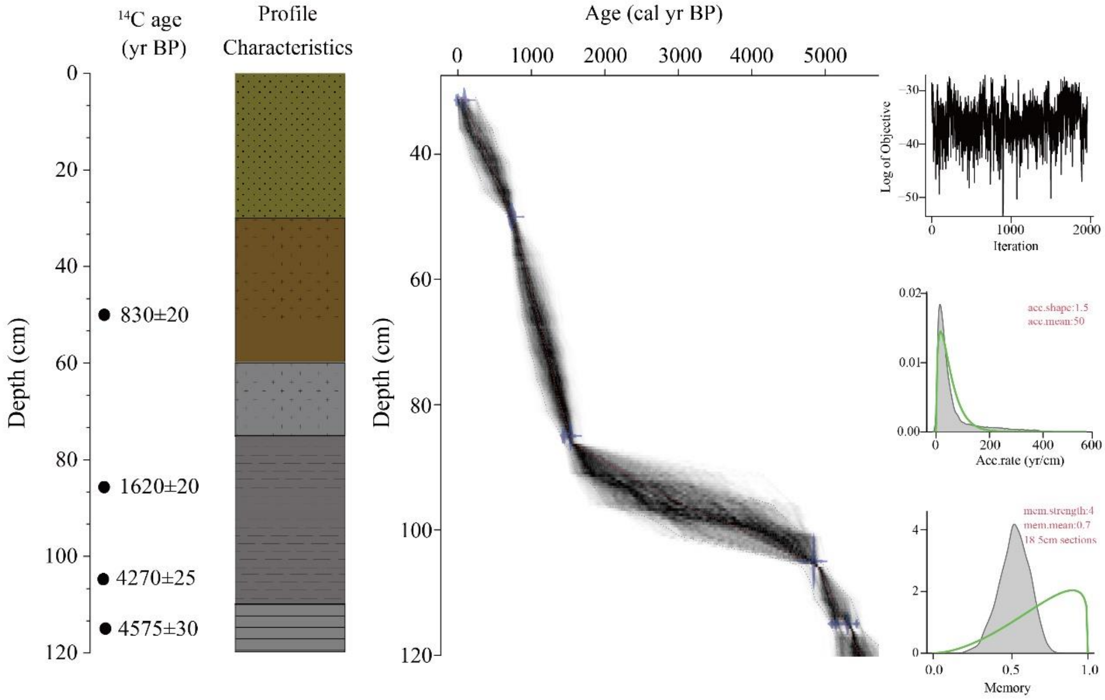

Fig.2. 'Bacon' age-depth models and accumulation rate for the Huanan peatland

Table 1 AMS radiocarbon dates of samples from the Huanan peatland

3.2.2 Grain size analysis

Laboratory code	Sample code	Depth interval (cm)	Sample type	AMS 14C (yr BP)	Calibrated date (2σ cal yr BP)
NENUR11088	HUA-50	50	Organic matter	830±20	790-682
NENUR11441	HUA-85	85	Organic matter	1620±20	1680-1406
AGE2024-0088	HUA-105	105	Organic matter	4270±25	4908-4486
NENUR11089	HUA-115	115	Organic matter	4575±30	5469-5075

We selected 90 samples in the 120-30 cm layer for grain size analysis. The extraction process of grain size was as follows: firstly, 3g of sample were weighted and placed in a 15 ml centrifuge tube; secondly, 10% HCl was added to remove carbonate. After washing to neutral with distilled water, 8 ml of H_2O_2 was added. After washing to neutral, 0.05 mol/L $(NaPO_3)_6$ was added and the sample vibrated ultrasonically; finally, grain sizes were measured with a Mastersizer 2000 laser at the School of Geography, Northeast Normal University. In order to reduce errors caused by uneven sampling, each sample was measured three times (Wang et al., 2022).

3.2.3 Total carbon, total nitrogen and carbon isotope analysis

In this paper, 45 samples were selected from the Huanan peatland at 2 cm intervals for measurement of chemical indicators. The experimental process was as follows: firstly, samples were dried and ground; then, 10% HCl was added to remove carbonate. After washing until neutral, total organic carbon content (TOC) and total nitrogen content (TN) and carbon isotopes ($\delta^{13}C$) were measured with an EURO VECTOR EA3000 elemental analyzer and a MAT-253 mass spectrometer. The samples were measured three times, and the final average was taken as the result (Guo et al., 2018).

3.2.4 Phytolith analysis

This paper selected 45 samples from the Huanan peatland at 2 cm intervals for phytolith analysis. Firstly, the sample was dried and 1 g weighed out; then, 10% HCL was added to remove carbonate; after washing to neutrality with distilled water, 5 ml of HNO_3 was added to remove organic matter; after washing to neutrality with distilled water, $ZnBr_2$ solution (specific gravity of 2.38 g cm^{-3}) was added; after cleaning with distilled water, one tablet containing a known number of 10315 *Lycopodium* spores was added, which was dissolved with an appropriate amount of 10% HCl; after washing with distilled water until neutral, 95% ethanol solution was added. Phytoliths were observed using an OLYMPUS BX53 biological microscope, and the number of phytoliths counted in each sample was not less than 300 (Gao, 2019).

3.3 Data analysis

Phytoliths are mainly classified and named according to the identification standards of ICPN2.0 (Neumann K et., 2019). The software used for phytolith analysis data processing was Tilia2.6.1, and the ordered clustering algorithm was calculated by the CONISS module that accompanies the Tilia2.6.1 software. In order to reconstruct the paleovegetation characteristics of the Huanan peatland quantitatively, we selected 99 topsoil samples from different forest areas in Northeast China as the reference data set (Changbai Mountain area, 49 samples; Lesser Khingan area, 29 samples; Greater Khingan area, 21 samples)（Gao et al., 2021）; the vegetation community numerical characteristics were reconstructed by partial least squares regression (PLS) analysis in C2 software. At the same time, we quantitatively reconstructed the coverage of tree cover and grass cover based on the random forest package in R 2022 software (Gao et al., 2022). In addition, we used software such as ArcGIS 2020, Ai 2022 and Origin 2022 to draw an overview map of the study area and the curves of other climate records. In addition, on the basis of phytolith taxonomic types, C3 and C4 plants can also be distinguished. C3 plants mainly include SADDLE and CRENATE types; C4 plants mainly include SADDLE, POLYLOBATE, CROSS and BILOBATE types (Neumann et al., 2017; Neumann et al., 2019). The forest-grass index (W/G) was calculated with reference to the formula proposed by Gao (Gao, 2019).

4. Results

4.1 Grain-size, total carbon, total nitrogen and carbon isotope characteristics

The Huanan peatland profile is characterized by a dominance of silt, followed by sand, and very low clay content (Fig. 3). Silt content ranges from 64.96% to 91.50% (average 15.91%), sand content ranges from 7.05% to 34.28% (average 81.77%), and clay content ranges from 0% to 8.29% (average 2.32%). The average sand content is 81.77%, with a median diameter (Md) range of 13.82 to 32.05 μm (average 20.38 μm). In the Huanan peatland profile over the past 5500 cal yr BP, Total Organic Carbon (TOC) fluctuated between 5.83% and 38.43% (average 22.76%), Total Nitrogen (TN) fluctuated between 0.5% and 3.71% (average 1.68%), and $\delta^{13}C$ ranged from -28.79‰ to -27.75‰ (average -28.14‰) (Fig. 3).

The profile can be divided into three stages: Stage I (5500-4000 cal yr BP) is mainly silt. Md is the coarsest in the profile during this stage, ranging from 13.82 to 32.05 μm (average 24.03 μm), peaking between 5500-5000 cal yr BP and decreasing after 5000 cal yr BP. Both TN and TOC remained at low levels, with values ranging from 0.5% to 1.53% (average

0.80%) and 5.83% to 19.31% (average 10.02%) respectively, while $\delta^{13}C$ remained negative between -28.32‰ and -27.76‰ (average -28.13‰). Around 4000 cal yr BP, there was a sudden increase in both TN and TOC, with TOC rising from 5% to 24%, TN increasing from 0.5% to 1.87%, and $\delta^{13}C$ becoming significantly positive, shifting from -28.15‰ to -27.78‰. Stage II (4000-1500 cal yr BP) is mainly silt with Md showing a coarsening trend during 4000-3200 cal yr BP, and then a fining trend during 3200-1500 cal yr BP. And it showed relatively smooth changes in TN, TOC, and $\delta^{13}C$. Stage III (1500-0 cal yr BP) is mainly silt with Md showing low values throughout the profile, ranging from 13.82 to 32.05 μm (average 18.71 μm), but the value range varies greatly. Between 600-400 cal yr BP, Md reaches its maximum value of 32.05 μm. Both TN and TOC exhibited a notable upward trend, reaching high values within the profile, with TN ranging from 1.31% to 3.71% (average 1.97%) and TOC from 12.22% to 38.43% (average 26.95%), while $\delta^{13}C$ was more negative, fluctuating between -28.79‰ and -27.75‰ (average -28.21‰).

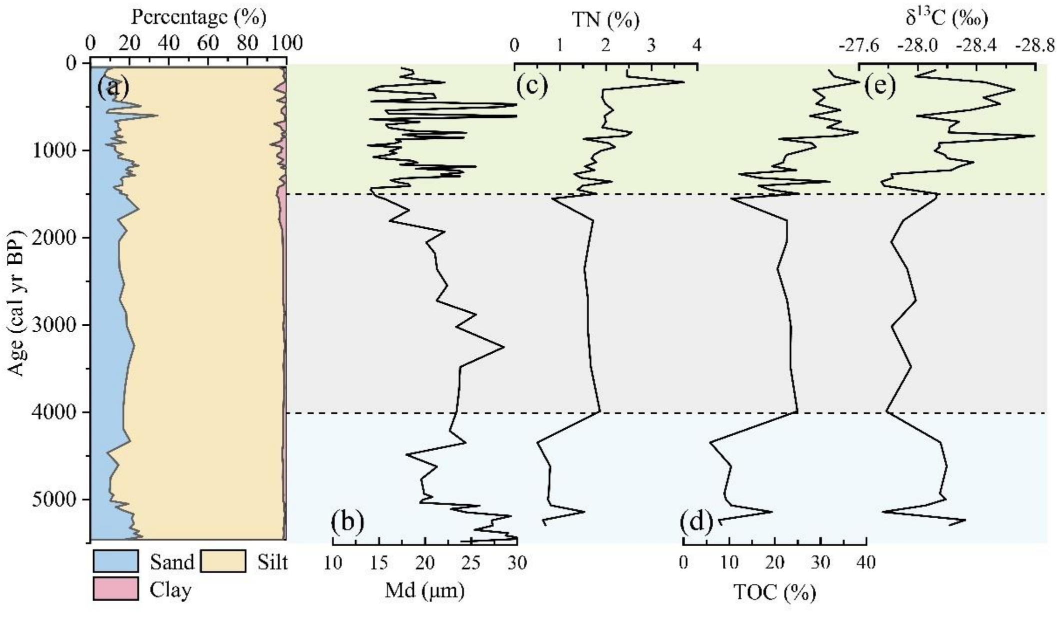

Fig. 3. Deposition characteristic of the Huanan peatland. (a) Grain size composition percentage; (b) Median diameter (Md); (c) Total nitrogen content (TN); (d) Total organic carbon content (TOC); (e) Carbon isotope ($\delta^{13}C$).

4.2 Late Holocene phytolith characteristics

The Huanan peatland profile is rich in phytolith species, and the concentration ranges from 7.58×10^4 to 6.75×10^6 grains g^{-1}, with an average of 2.57×10^6 grains g^{-1} (Fig. 4). According to the ordered clustering algorithm of phytolith assemblage, profile lithological characteristics and climate index results, the Huanan peatland profile is divided into three zones (Fig. 4). Combining the reconstructed plant community coverage, species diversity, grass cover, tree cover, C3/(C3+C4) radio, and the forest-grass index (W/G) index (Fig. 5), the vegetation community numerical characteristics in Huanan peatland during the Late Holocene were as described in the following paragraphs.

The community coverage ranges from 56.74 to 74.00%, with an average value of 66.53%, while species diversity ranges from 0.53 to 0.77, averaging at 0.62, both showing a declining trend. Tree cover and the W/G index exhibit a similar increasing trend, with ranges of 22.44~32.72% and 0.03~0.30 respectively. Grass cover remains relatively stable, varying from 37.94 to 48.14%, with an average of 43.71%. C3 herbaceous plants are predominant, but their proportion is decreasing, and $\delta^{13}C$ ranges from -28.79 to -27.75‰, averaging at -28.18‰.

In Zone I (2000-1300 cal yr BP), the phytolith concentration ranged from 2.96×10^5 to 5.90×10^6 grains g-1, with an average of 2.81×10^6 grains g-1. The highest phytolith concentration was observed in the section, mainly consisting of CRENATE, ELONGATE and LANCEOLATE types. Community coverage and species diversity varied between 59.76 to 70.67% and 0.52 to 0.67 with average values of 67.68% and 0.64, which were the highest in the profile. Community coverage exhibited a decreasing trend, while species diversity showed a slight increase. Tree cover and the W/G index were the lowest, ranging from 24.18 to 28.94% and 0.04 to 0.10, respectively, with a slight downward trend. Grass cover remained relatively stable, ranging from 37.94 to 46.80%. The C3/(C3+C4) ratio indicated a higher proportion of C3 herbaceous plants in the profile, showing a gradual increase. The $\delta^{13}C$ values were positive, ranging from -28.13 to -27.75‰.

In Zone II (1300-750 cal yr BP), phytolith concentration decreased compared with the previous zone, ranging from 8.44×10^5 to 6.75×10^6 grains g^{-1}, with an average of 2.81×10^6 grains g^{-1}. Community coverage and species diversity ranged from 56.74 to 74.00% and 0.53 to 0.72, with average values of 66.70% and 0.62 respectively. Both average values declined compared to the previous zone, with an increase in community coverage between 1100 and

900 cal yr BP, while species diversity showed a downward trend. Tree cover and the W/G index showed a clear upward trend, ranging from 22.44% to 30.81% and 0.025 to 0.25. The average values increased compared to the previous zone, reaching 26.12% and 0.11 respectively. Grass cover remained relatively stable, with only a slight decrease compared to the previous zone. The proportion of C3 herbaceous plants remained the highest in the profile, but the C3/(C3+C4) ratio showed a gradual decrease. In comparison to the previous zone, there was a noticeable negative in $\delta^{13}C$ values, ranging from -28.79‰ to -27.82‰.

In Zone III (750-0 cal yr BP), the phytolith concentration continued to decrease, reaching its lowest level in the profile, ranging from 7.58×10^4 to 6.17×10^6 grains g-1, with an average value of 2.09×10^6 grains g-1. Community coverage and species diversity ranged from 59.76 to 70.67% and 0.53 to 0.68, with average values of 65.41% and 0.61 respectively. In comparison to the previous zone, both average values continued to decline, with an initial increase followed by a decreasing trend. Tree cover and the W/G index showed an overall increase compared with the previous zone, ranging from 24.09 to 32.72% and 0.03 to 0.30 respectively, but with a low point during 500 to 300 cal yr BP. Grass cover dropped slightly on average compared to the previous zone, but remained relatively stable. C3 herbaceous plants still dominated the profile, with $\delta^{13}C$ values negatively skewed compared to the previous zone, ranging from -28.66 to -27.98‰.

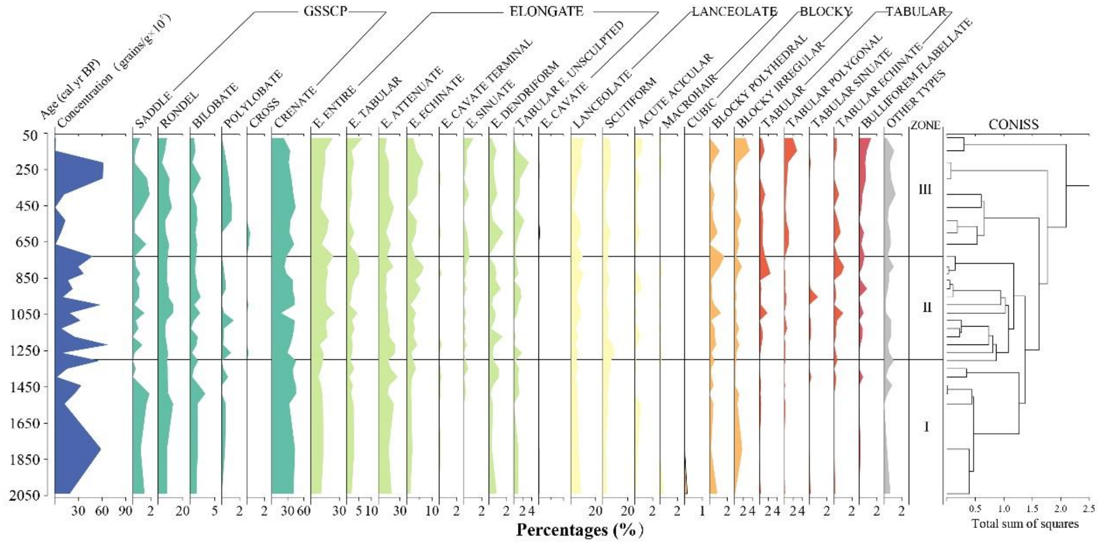

Fig. 4. Phytolith assemblages and results of stratigraphically constrained cluster analysis of the Huanan peatland

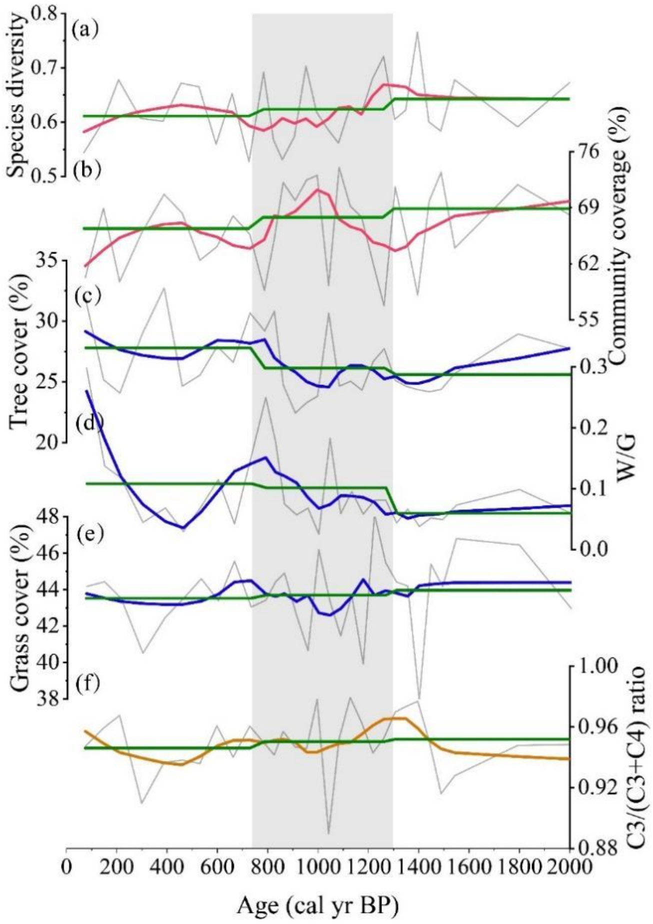

Fig. 5. The phytolith-based paleovegetation reconstruction results in Huanan peatland. (a) Species diversity; (b) Community coverage; (c) Tree cover; (d) The forest-grass index (W/G) index; (e) Grass cover; (f)C3/(C3+C4) ratio (Green lines refer to the mean value of each layer).

5. Discussion

5.1 The evolution of peatlands

Changes in TOC and TN contents in different depths of peatland sediments, as well as grain size and distribution characteristics of grain size, can provide insights into the evolution and accumulation process of peatland (Visher, 1969; McLaren and Bowles, 1985). Peat deposition is commonly characterized by TOC content of over 15% (Chai, 1990). Zhang et al. (2019) found that in the Jinchuan peatland sediments of the Changbai Mountains, the TOC and TN of peatland sediments are usually higher than 20% and 1.5%, respectively, whereas lake sediments exhibit lower levels (Zhang et al., 2019). Based on the division criteria of TOC and TN values, the transition from lake to peatland is identified at 105 cm depth, marking the initiation of Huanan peatland formation around 4000 cal yr BP. The grain-size characteristics of peat ash and frequency distribution curves are sensitive to different sedimentary conditions and can also indicate the developmental history of the Huanan peatland. However, the grain-size characteristics of sediments have been interpreted differently in different studies. For example, Zhang et al. (2014) concluded that during the development of the lake, as the water level rises in the central profile of the lake, the hydrodynamic force weakens, facilitating the settlement of the fine component and a reduction in sediment grain size. Dong et al. (2022) concluded that the grain size of lake sediments found on the shore of Bosten Lake is indicative of the hydrodynamic conditions of the lake. A rise in the lake's water level will result in an increased proportion of the coarser component in the sediment and an increase in sediment grain size (Dietze et al., 2013; Lu et al., 2018; Dong et al., 2022). Therefore, the relationship between grain size and water level needs to be specifically explained by analyzing different sedimentary environments (Dietze et al., 2013; Lu et al., 2018; Vandenberghe et al., 2018). Huanan peatland is situated on the floodplain of small rivers, where the grain size of debris particles is highly influenced by water level fluctuations. Increased precipitation and rising river water levels result in increased hydrodynamic force, allowing coarse-grained matter to be transported to the peatland, thereby increasing peat ash grain size. Conversely, when river water levels decrease, the carrying capacity of flowing water weakens, making it difficult for coarse-grained matter to reach the sampling point and causing peat ash particles to become finer (Elizabeth et al., 2020).

Therefore, the grain size, TOC and TN results in this study indicate that the development of Huanan peatland may have been influenced by regional climate change and local hydrological environmental conditions, potentially transitioning from lakes (Fig. 6).

During 5500-4000 cal yr BP, the East Asian summer monsoon (EASM) exhibited strength, resulting in heightened regional precipitation. This led to elevated river water levels in the Huanan peatland, causing flooding in the floodplain and the formation of lakes. These conditions were not conducive to the development of peatland. During this time, the Huanan sediment displayed a blue-gray hue, with coarser peat ash grain size that was highly sensitive to changes in the sedimentary environment. The frequency distribution curves of sediment grain size varied under different sedimentary conditions. When the river water level caused submergence of the Huanan peatland, sampling points located far from the shore experienced weak hydrodynamic conditions, resulting in a unimodal state in the grain size frequency distribution curve. It is hypothesized that this state was solely influenced by the hydrodynamic conditions of the lake during this period (Zhang et al., 2020). The average values of TOC and TN are both low, with 8.70% and 0.80% respectively. The flooded anaerobic environment does not support the accumulation of peatland organic matter. At this time, the Huanan sediments may be lacustrine deposits.

During 4000-1500 cal yr BP, the EASM weakened, leading to a trend towards arid conditions. Pollen records from Sihailongwan and Xiaolongwan, peat ash grain size data from Gushantun and Hani, and carbon isotope analysis from Xingkai Lake all indicate a significant decrease in regional precipitation since 4000 cal yr BP (Stebich et al., 2015; Li et al., 2017; Xu et al., 2019). The positive $\delta^{13}C$ values of peatland sediments in Huanan indicate that regional climate change is influencing this area, leading to a trend towards arid conditions. The water level in the peatland has decreased. Huanan peatland may be flooded only occasionally by seasonal precipitation. At this time, the peatland layer exhibited a gray-black color, with a finer grain size and a bimodal pattern in the grain size frequency distribution curve. These observations indicate that sedimentation processes may be influenced by both the hydrodynamic conditions of the lake and seasonal rivers (Zhang et al., 2020). The TOC and TN values of Huanan peatland showed a significant increase, with the TOC value rising from 5% to 24% and the TN value increasing from 0.5% to 1.87%. These changes suggest that peatland accumulation has commenced. During the lake swampization process, peat formation occurred during a drier climatic compared to the preceding stage. A similar phenomenon was also observed in the Jinchuan and Gushantun peats within the Changbai Mountains (Zhang et al., 2020, 2021).

After 1500 cal yr BP, the EASM has weakened, leading to decreased regional precipitation and a persistently dry climate with lower river water levels. The $\delta^{13}C$ of peat deposits in Huanan has stabilized at a high level, suggesting a significant increase in aridity compared to the previous period. The peatland may remain isolated from changes in river levels over extended periods. During this time, the peat layer appears grayish brown, with a coarser Md and a particle size frequency distribution curve showing double peaks, indicating deposition possibly influenced by both wind and flowing water simultaneously (Visher, 1969). Additionally, the average TOC and TN values were recorded at 24.29% and 1.78% respectively, reaching peak levels in the profile. This shows that peat accumulated steadily at this time, and the sedimentation rate reached the highest value in the profile, 0.039 cm/yr. The carbon burial capacity and carbon sink function of peatland are enhanced.

It is worth noting that the peat accumulation rate is influenced by various factors including climate conditions, vegetation composition, and local topography (Charman et al., 2015; Mathijssen et al., 2016; Gallego-Sala et al., 2018). However, it is primarily linked to plant production and decomposition intensity (Chai, 1990). In warm and humid climates, plant decomposition rates accelerate, whereas in cold and dry climates, plant production decreases, affecting the rate of peat accumulation. Research indicates that peatlands in the Changbai Mountains have a peat accumulation rate ranging from 0.3-1.2 mm/a, while in this study the rate at the initial development stage of Huanan peat was only 0.075 mm/a (Zhao et al., 2002; Dong et al., 2023). The low peat accumulation rate in Huanan peatland can be attributed to fluctuations in local water levels. The Huanan peatland profile is located on the floodplain of the Xiaobahuli River, with small rivers developing around it. It is located in an intermountain valley and is a relatively low-lying landform unit. Water primarily enters the area through rivers, slope runoff, and groundwater, causing water level variations in the peatlands that are typically influenced by regional precipitation. For example, during the high water level period from 4000 to 1500 cal yr BP, vegetation on the Huanan peatland was sparse, biomass accumulation was slow, and the peatland remained in an anaerobic environment for an extended period. This led to sluggish peat development and, in some cases, stagnant peat growth (Afify et al., 2022).

In the future, as global warming and human activities intensify, the peatlands in Changbai Mountain are likely to face widespread destruction and degradation (Liu et al., 2024). This transformation may cause these peatlands to shift from being significant carbon sinks to major carbon sources (Evans et al., 2022). Therefore, the protection of peatlands and the restoration of degraded peatlands in Northeast China should be strengthened.

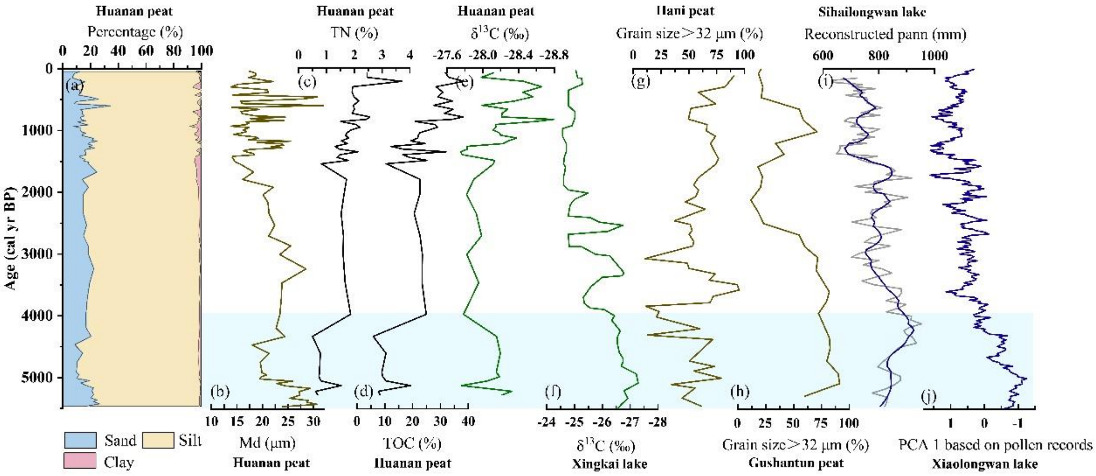

Fig. 6. Deposition characteristics of the Huanan peatland core and comparison with other records. (a) Grain size composition percentage of the Huanan peatland profile (this study); (b) Median diameter (Md) of the Huanan peatland profile (this study); (c) Total nitrogen content (TN) of the Huanan peatland profile (this study); (d) Total organic carbon content (TOC) of the Huanan peatland profile (this study); (e) Carbon isotope ($\delta^{13}C$) of the Huanan peatland profile (this study); (f) $\delta^{13}C_{org}$ (‰) records in Xingkai Lake (Wu et al., 2010); (g) Percent of grain size >32 μm in Hani peatland (Li et al., 2017); (h) Percent of grain size >32 μm in Gushantun peatland (Li et al., 2017); (i) Annual rainfall based on pollen records in Sihailongwan Lake (Stebich et al., 2015); (j) PCA F1 samples scores based on pollen analysis in Xiaolongwan Lake (Xu et al., 2019).

5.2 Reconstruction of Huanan peatland paleovegetation

Scholars initially developed a semi-quantitative method for reconstructing paleovegetation using multiple phytolith indices to analyze forest coverage in phytolith assemblages. Commonly utilized phytolith indices include the D/P, Pi/P, and the W/G index (Alexandre et al., 1997; Delhon et al., 2003; Gao, 2019). Owing to the variation in types of phytoliths across regions, the phytolith index has different applications in different areas. The first two indices are mainly used in tropical regions and Mediterranean areas, whereas the W/G index is more effective for identifying typical vegetation types and various types of grassland and forest communities in Northeast China. This index allows for semi-quantitative differentiation of vegetation types (Gao, 2019). On this basis, Gao et al. (2022) utilized the relationship between topsoil phytolith assemblage and vegetation covering the peatland to reconstruct tree cover and grass cover quantitatively using the random forest method. Additionally, phytoliths have been found to be advantageous for the recording of understory grasses. Previous studies have shown that the Ic index can indicate changes in the relative amounts of C3 and C4 herbaceous plants (Bremond et al., 2008), and it has been deemed applicable in the Northeast China region as well (Yang et al., 2023).

This study selects the late Holocene as the research period to reconstruct the paleovegetation of the Huanan peatland. Mainly based on the following three reasons. Firstly, during the period of 5500-2000 cal yr BP, the Huanan peatland underwent lake swamping, characterized by low sample deposition rates and temporal resolution and developed into typical peat after 2000 cal yr BP. Secondly, during the period of 5500-2000 cal yr BP, regional precipitation increased (Stebich et al., 2015; Xu et al., 2019), leading to elevated river levels. The sediment sources in the Hunan peatland were complex (Swinnen et al., 2021), and the origins of phytoliths remained ambiguous, which contributed to inaccuracies in the reconstruction of paleovegetation (Garnier et al., 2013; Barros et al., 2016). Thirdly, between 5500 and 2000 cal yr BP, the sediment grain size was coarser and the phytolith concentration was lower than in the period following 2000 cal yr BP, rendering it unsuitable for reconstructing vegetation changes.

Research on the use of phytoliths to reconstruct past vegetation types is gradually progressing. Current investigations have advanced from qualitative and semi-quantitative approaches to a quantitative methodology for reconstructing paleovegetation changes (Gao et al., 2021). Research on the use of phytoliths to reconstruct past vegetation types is gradually progressing. Based on the results of phytolith analysis, previous studies have demonstrated that when the reconstructed tree cover exceeds 23.7%, there is a high probability that the primary vegetation type in the area is a forest community (Gao et al., 2022). The findings of this article meet this criterion (Fig. 7). However, in comparison to other sections within the forest area, the forest and grass index reconstructed from phytoliths indicates that the W/G index in the forest area typically remains above 0.4 (Gao, 2019), while the W/G index reported in this paper is lower than 0.23 for most periods. This discrepancy may be attributed to the fact that, although the overall vegetation in this area is primarily composed of forest communities, the phytoliths still accurately capture the information about the herbaceous communities around the peatland during part of the period. Concurrently, pollen analysis from the Hunan peat profile revealed that sedge pollen dominated the herbaceous plant pollen, suggesting the presence of meadow grasslands on the Huanan peatland (Jie et al., 2012). Additionally, woody pollen types, including Betula and Quercus, were relatively abundant (Jie et al., 2012). The higher abundance of these pollen types indicates that the regional vegetation is likely a mixed coniferous and broad-leaved forest, which aligns with the vegetation information reconstructed from phytoliths. In summary, from the perspective of the evolution history of vegetation types, the main vegetation type in the Huanan area since 2000 cal yr BP has been forest vegetation, and the surrounding peatlands have been herbaceous communities in part of the period.

In addition, the Shenjiadian peatland in the Sanjiang Plain, located 22 km from the Hannan peatlland, is situated in mountainous valleys with a comparable local environment and climatic background. The extant vegetation types in this area are similar to those found in the Hannan peatland. Plant macrofossil evidence from the Shenjiadian peatland section indicates a prevalence of Poaceae since 3800 cal yr BP, indicating a grassland ecosystem (Wang et al., 2015). In contrast, according to the pollen analysis results of the Mishan Yangmu profile in the Sanjiang Plain, the regional vegetation has been mixed coniferous and broad forests since 2000 cal yr BP , similar to the findings of this study (Xia et al., 2000). Although there were some changes in community coverage during the middle and late Holocene, no significant shifts in species types were detected, and species diversity remained relatively stable. Similar trends have been observed in the Hani peatlands of the Changbai Mountains (Gao et al., 2021).

Previous studies have demonstrated that phytoliths can serve as valid indicators for changes of the C3 to C4 plants ratios and have been used in various regions worldwide (Twiss et al., 1992; Alexandre et al., 1997; Blinnikov et al., 2002; Barboni et al., 2007; Crifò et al., 2023) and in northeastern China (Li et al., 2017; Gao et al., 2021). In this study, phytoliths can reconstruct the relative plant numerical characteristics of C3/C4 in herbaceous plants (Fig. 7). This is a big advance over pollen analysis, which cannot provide such information. The results of phytoliths and $\delta^{13}C$ both indicate that during the Holocene, the Huanan peatland was dominated by C3 herbaceous plants while the proportion of C4 herbaceous plants was relatively less. The results of the reconstruction of the two indicators differed only for part of the period. For example, in 750-0 cal yr BP, when $\delta^{13}C$ was the most negative, the C3 herbaceous plants reconstructed by phytoliths were at their low value in the profile; while in the 2000-1300 cal yr BP, when $\delta^{13}C$ was more positive, the phytoliths indicate the C3 herbaceous plants are at their high value in the profile. The reason for this difference is mainly due to the representative difference of indicators for vegetation. When using phytolith assemblage for restoration, the focus is on the quantity change of C3 and C4 herbaceous plants in the forest understory, whereas $\delta^{13}C$ analysis provides information on all woody and herbaceous plants. Since most of the woody plants are C3 plants, when the woody plants decline, it will cause a positive δ13C without causing changes in the phytoliths (Twiss, 1992; Fredlund et al., 1994; Bremond et al., 2008).

5.3 Vegetation dynamics response to climate changes

Previous studies have indicated that Holocene temperature changes in the Northeast China are relatively uniform, aligning with variations in solar radiation Northern Hemisphere. The principal discrepancies are concentrated in humidity and precipitation (Hong et al., 2001, 2003, 2009; Zheng et al., 2017). In this manuscript, the use of a single grain size to indicate changes in paleoclimate primarily focuses on reconstructing humidity variations around Huanan peatlands, while not adequately addressing temperature changes in the region owing to the relatively uniform temperature changes in the Northeast China. Based on the EASM index and regional climate records (Kang et al., 2020; Niu et al., 2024), it has been observed that from 2000-750 cal yr BP, solar radiation gradually weakened, leading to a decline in the EASM and a gradual cool and dry of the climate in Northeast China (Fig. 7). The EASM strengthened after 750 cal yr BP, and the climate in Northeast China was warmer and wetter than the previous period. Huanan peatland inorganic sediments are primarily sourced from river transport, with the size of peatland grains being influenced by flow dynamics (Li et al., 2017). This makes them a reliable indicator of dry and wet fluctuations in paleoenvironmental changes, serving as a proxy for variations in paleoprecipitation or summer monsoon intensity (Qu et al., 2024). The trend in Md is consistent with the summer monsoon curve, providing further evidence to support this hypothesis. The Huanan peatland more realistically records the information of the natural section, and the evolution dynamics of ancient vegetation are similar to climate change trends, indicating that climate factors are the most important factors affecting vegetation change (Zhao et al., 2012).

During the period of 2000-1300 cal yr BP, there was a rapid decline in the EASM, leading to a regional climate shift from warm and humid to cold and dry (Niu et al, 2024). This environmental change is consistent with the findings of this study, which used grain size analysis to reconstruct the environmental history of the Huanan peatland. This trend is also reflected in the temperature and precipitation curves reconstructed from pollen data in Sihailongwan (Stebich et al., 2015). The study observed high community coverage and species diversity of Huanan peatland vegetation during this time, with well-developed herbaceous plants, particularly C3 herbaceous plants. In contrast, the number of regional woody plants was relatively small and exhibited a gradual decline. It is worth noting that the study's reconstruction of the changing numerical characteristics of woody plants based on phytoliths primarily reflects regional vegetation changes rather than local vegetation changes specific to the Huanan peatland. The main reason is that the woody phytoliths in the Huanan peatland may have been formed by wind and water forces that carried surrounding leaves here (Fredlund et al., 1994; Fredlund et al., 1997).

During the period 1300-750 cal yr BP, the EASM exhibited a gradual decline, leading to a regional climate characterized by cold and dry conditions (Niu et al., 2024). However, the Md of the Huanan peat ash actually increased during this time frame. Precipitation records from Sihailongwan also increased during this period (Stebich et al., 2015). This suggests a rise in river water level, indicating higher precipitation in the river basin compared to the preceding period. At this time, owing to the partial and intermittent submergence of the peatland, the community coverage and species diversity of local vegetation in the Huanan peatland decreased, the grass cover decreased, and the $\delta^{13}C$ value became significantly negative, suggesting a notable increase in C3 plants. Additionally, the regional tree cover was influenced by increased precipitation, showing an upward trend.

After 750 cal yr BP, the EASM intensified (Chen et al., 2008; Kang et al., 2020), leading to a warmer and more humid regional climate (Niu et al, 2024). The Md of Huanan peat ash increased compared with the previous period, and the local climate changes were consistent with the regional climate. The $\delta^{13}C$ value of the Huanan peatland became more negative, suggesting an increase in regional tree cover. However, local grass cover, community coverage, and species diversity all experienced a decline. This phenomenon can be attributed to two main reasons. Firstly, the decrease in solar radiation and precipitation reaching understory herbaceous plants after an increase in tree cover may restrict herbaceous plants growth (Chamagne et al., 2016). Secondly, it may be due to the coarsening of grain size and the rise of river water levels that the Huanan peatland is intermittently flooded by seasonal flowing water, resulting in a decrease in local grass cover (Fletcher et al., 2000).

The regional and local vegetation of the Huanan peatland is not only affected by long-term climate change, but is also sensitive to the response to climate events. For example, during the Medieval Warm Period, the EASM exhibited strength (Kang et al., 2020), leading to a warm and humid regional climate (Niu et al., 2024). Throughout this time, the Md of the Huanan peat ash experienced an increase, albeit remaining relatively low c. 2000 cal yr BP. This suggests a gradual shift in the local climate from cold and dry conditions to warmer and more humid conditions. In response to the regional warm and humid climate, the regional tree cover increased. However, the grass cover only slightly increased, while the overall community coverage and species diversity decreased. This could be due to the low water level in the Huanan peatland, which limits vegetation growth (Breeuwer et al., 2009). During the Little Ice Age, the EASM weakened, leading to a regional climate shift from warm and humid to cold and dry. The Md of Huanan peatland decreased, indicating that the local climate gradually became cold and dry. Additionally, a decrease in regional tree cover was observed. Corresponding to the local climate change trend, it was reflected in the decline of local grass cover, overall community coverage, and species diversity.

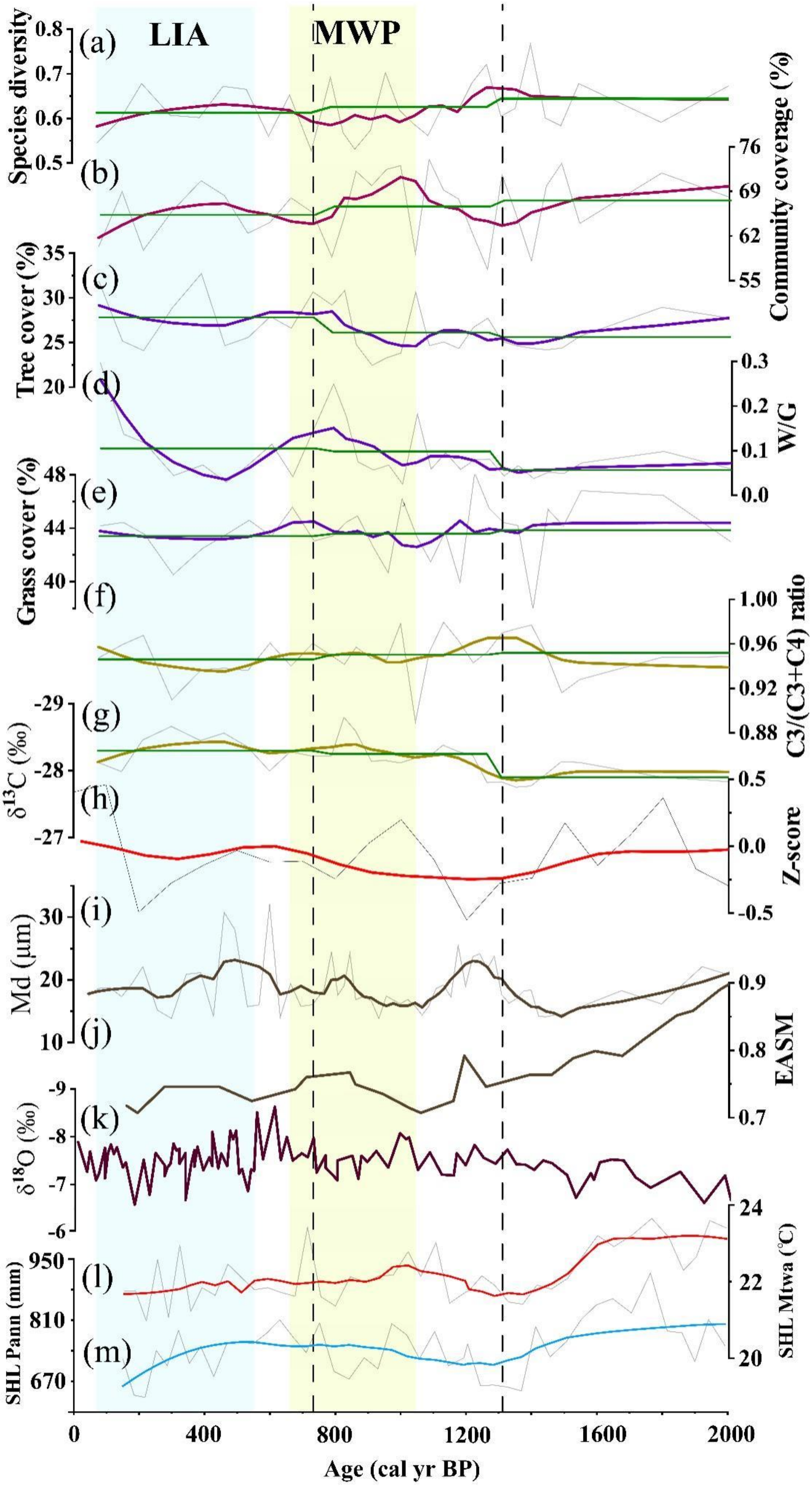

LIA
MWP
Species diversity
Community coverage (%)
Tree cover (%)
W/G
Grass cover (%)
C3/(C3+C4) ratio
δ13C (‰)
Z-score
Md (μm)
EASM
δ18O (‰)
SHL Pann (mm)
SHL Mtwa (℃)
Age (cal yr BP)

Fig. 7. The phytolith-based paleovegetation reconstruction and comparison with other records. (a) Species diversity of the Huanan peatland profile (this study); (b) Community coverage of the Huanan peatland profile (this study); (c) Tree cover of the Huanan peatland profile (this study); (d) The forest-grass index (W/G) index of the Huanan peatland profile (this study); (e) Grass cover of the Huanan peatland profile (this study); (f) C3/(C3+C4) ratio of the Huanan peatland profile (this study); (g) Carbon isotope ($\delta^{13}C$) of the Huanan peatland profile (this study); (h) Z-score calculated based on selected climate records in Northeast China (Niu et al., 2024); (i) Median diameter (Md) of the Huanan peatland profile (this study); (j) East Asian Summer Wind Intensity (Kang et al., 2020); (k) Composited stalagmite δ18O scores in northeastern Asia (Zhao et al., 2021); (l) Annual rainfall based on pollen records in Sihailongwan Lake (Stebich et al., 2015); (m) Mean warmest month (July) temperature on pollen records in Sihailongwan Lake (Stebich et al., 2015) (Green lines refer to the mean value of each layer).

6. Conclusion

This study focuses on the Huanan peatland section in the Changbai Mountain regions of Northeast China, utilizing phytolith analysis and stable carbon isotope composition ($\delta^{13}C$) to reconstruct the numerical characteristics of the vegetation community during the late Holocene. In addition, the research investigates the development and evolution of the Huanan peatland and regional paleoclimate changes by analyzing grain size, total organic carbon content (TOC), and total nitrogen content (TN). The results show that since 5500 cal yr BP, the climate of the Huanan peatland has undergone significant changes that have influenced both vegetation dynamics and peatland development.

In terms of the peatland development process, from 5500-4000 cal yr BP, the climate was warm and humid, leading to the deposition of coarser peat ash grain sizes. During this time, strong regional precipitation caused river levels to rise, submerging the peatland and resulting in the formation of lacustrine sediments. Between 4000-1500 cal yr BP, the climate transitioned from warm and humid to cold and dry, which corresponded with a finer grain size in the peat ash. The reduction in precipitation led to a drop in river levels, allowing the peatland to begin developing. Finally, from 1500 cal yr BP to the present, the climate remained cold and dry, with peat ash grain size reaching its minimum. Despite a continued decrease in regional precipitation and river water levels, peat development persisted steadily. This sequence underscores the closely linked relationship between climate change and peatland evolution over time.

The vegetation-climate interaction in this region can also be divided into three distinct periods: from 2000-1300 cal yr BP, the climate transitioned from warm and wet to cold and dry, leading to dense vegetation with diverse species, including well-developed herbaceous plants and a relatively high number of regional herbaceous species. Between 1300-750 cal yr BP, as the climate remained cold and dry, plant community coverage and species diversity declined, with a noticeable decrease in grass cover. However, regional tree cover increased due to a slight rise in precipitation. Finally, from 750-0 cal yr BP, the climate became warm and humid, resulting in an increase in regional woody plant cover. Despite this shift, local grass cover, overall plant community coverage, and species diversity continued to decline.

The integrated approach used in this study provides a comprehensive understanding of the interconnectedness between climate change, peatland evolution, and vegetation dynamics. These findings offer a valuable framework for reconstructing paleoenvironmental changes in other regions as well.

Acknowledgements

This work was supported by the Natural Science Foundation of Jilin Province (Award 20220101149JC, 2412021ZD005), the National Natural Science Foundation of China (Grant/Award Numbers: 42271162, 41971100) and the National Cultural Heritage Administration (Grant/Award Numbers: 2023ZCK012).

References

Afify, A.M., Sanz-Montero, M.E., González-Acebrón, L., Muñoz-García, M.B., 2022. Sedimentary evolution of tectonically-controlled Cenozoic shallow marine glaucony, fluviatile and lacustrine-palustrine deposits at Bahariya region, Egypt. J. Afr. Earth Sci. 190, 104525.

Alexandre, A., Meunier, J.D., Lézine, A.M., Vincens, A., Schwartz, D., 1997. Phytoliths: indicators of grassland dynamics during the late Holocene in intertropical Africa. Palaeogeogr. Palaeoclimatol. Palaeocol. 136, 213-229.

Barboni, D., Ashley, G.M., Rodrigo, M.D., Bunn, H.T., Mabulla, A.Z.P., Baquedano, E., 2010. Phytoliths infer locally dense and heterogeneous paleovegetation at FLK north and surrounding localities during upper bed I time, Olduvai Gorge, Tanzania. Quat. Res. 74, 344-354.

Barboni, D., Bremond, L., Bonnefille, R., 2007. Comparative study of modern phytolith assemblages from inter-tropical Africa. Palaeogeography, Palaeoclimatology, Palaeoecology, 246, 454-470.

Barros, L.F.P., Coe Gomes, H.H., Seixas, A.P., Magalhães Jr., A.P., Macario, K.C.D., 2016. Paleobiogeoclimatic scenarios of the late quaternary inferred from fluvial deposits of the Quadrilátero Ferrífero (southeastern Brazil). Journal of South American Earth Sciences, 67, 71-88.

Blinnikov, M., Busacca, A., Whitlock, C., 2002. Reconstruction of the late Pleistocene grassland of the Columbia basin, Washington, USA, based on phytolith records in loess. Palaeogeogr. Palaeoclimatol. Palaeocol. 177, 77-101.

Breeuwer, A., Robroek, B.J.M., Limpen, J., Heijmans, M.M.P.D., Schouten, M.G.C., Berendse, F., 2009. Decreased summer water table depth affects peatland vegetation. Basic Appl. Ecol. 10, 330-339.

Bremond, L., Alexandre, A., Peyron, O., Joel, G., 2008. Definition of grassland biomes from phytoliths in West Africa. J. Biogeogr. 35, 2039-2048.

Cai, C., Hong, B., Zhu, Y.X., Hong, Y.T., Wang, Y., Peng, H.J., 2013. Holocene peat accumulation rates and influence factors from the Hani peatland, northeast China (in Chinese). Earth. Environ. 41, 597-604.

Chai, X., 1990. Peat Geology (in Chinese). Beijing: Science Press. 1-116.

Chamagne, J., Paine, C.E.T., Schoolmaster, D.R., Jr., Stejskal, R., Volařík, D., Šebesta, J., Trnka, F., Koutecký, T., Švarc, P., Svátek, M., Hector, A. and Matula, R., 2016. Do the rich get richer? Varying effects of tree species identity and diversity on the richness of understory taxa. Ecology 97, 2364-2373.

Charman, D.J., 2002. Peatlands and environmental change. Geoarchaeology 19 (4), 0-337.

Charman, D.J., Amesbury, M.J., Hinchliffe, W., Hughes, P.D.M., Mallon, G., Blake, W.H., Daley, T.J., Gallego-Sala, A.V., Mauquoy, D., 2015. Drivers of Holocene peatland carbon accumulation across a climate gradient in northeastern North America. Quat. Sci. Rev. 121, 110-119.

Charman, D.J., Amesbury, M.J., Hinchliffe, W., Hughes, P.D.M., Mallon, G., Blake, W.H., Daley, T.J., Gallego-Sala, A.V., Mauquoy, D., 2015. Drivers of Holocene peatland carbon accumulation across a climate gradient in northeastern North America. Quat. Sci. Rev. 121, 110-119.

Chen, F.H., Yu, Z.C., Yang, M.L., Ito, E., Wang, S.M., Madsen, D.B., Huang, X., Zhao, Y., Sato, T., Birks, H., Boomer, I., Chen, J., An, C., Wubbemann, B., 2008. Holocene

moisture evolution in arid central Asia and its out-of-phase relationship with Asian monsoon history. Quat. Sci. Rev. 27 (3-4), 351-364.
Crifò, C., Berrio, J.C., Boom, A., Giraldo-Cañas, D.A., Bremond, L., 2023. A paleothermometer for the northern Andes based on C3-C4 grass phytoliths. Paleobiology, 49 (3):414-430.
Delhon, C., Alexandre, A., Berger, J.F., Thi´ ebault, S., Brochier, J.L., Meunier, J.D., 2003. Phytolith assemblages as a promising tool for reconstructing Mediterranean Holocene vegetation. Quat. Res. 59, 48-60.
Dietze, E., Maussion, F., Ahlborn, M., Diekmann, B., Hartmann, K., Henkel, K., Kasper, T., Lockot, G., Opitz, S., Haberzettl, T., 2013. Sediment transport processes across the Tibetan Plateau inferred from robust grain size end-members in lake sediments. Clim. Past 9, 4855-4892.
Dingle, E.H., Sinclair, H.D., Venditti, J.G., Attal, M., Kinnaird, T.C., Creed, M., Quick, L., Nittrouer, J.A., Gautam, D., 2020. Sediment dynamics across gravel-sand transitions: Implications for river stability and floodplain recycling. Geology 48 (5), 468-472.
Dong, Y., Li, H., Wang, S., He, H., 2023. The development process of a temperate montane peatland and its controlling factors since the middle Holocene. Sci. China Earth Sci. 66 (3), 594-608.
Dong, Y.M., Li, H.K., He, H.S., Wang, S.Z., 2022. The persistent lake level decreasing induced Phragmites peatland development in the Bosten Lake (Northwest China) during the Medieval Warm Period. Quat. Int. 625, 38-48.
Evans, M. G., Alderson, D. M., Evans, C. D., Stimson, A., Allott, T. E. H., Goulsbra, C., Worrall, F., Crouch, T., Walker, J., Garnett, M., Rowson, J., 2022. Carbon loss pathways in degraded peatlands: New insights from radiocarbon measurements of peatland waters. Journal of Geophysical Research: Biogeosciences, 127, e2021JG006344.
Fletcher, D.E., Wilkins, S.D., McArthur, J.V., Meffe, G.K., 2000. Influence of riparian alteration on canopy coverage and macrophyte abundance in Southeastern USA blackwater streams. Ecol. Eng. 15, 67-78.
Fredlund, G.G., Tieszen, L. T., 1994. Modern Phytolith Assemblages from the North American Great Plains. J. Biogeogr. 21 (3), 321.
Fredlund, G.G., Tieszen, L.L., 1997. Calibrating grass phytolith assemblages in climatic terms: Application to late Pleistocene assemblages from Kansas and Nebraska. Palaeogeogr. Palaeoclimatol. Palaeoecol. 136 (1-4), 199-211.
Fredlund, G.G., Tieszen, L.T., 1994. Modern Phytolith Assemblages from the North American Great Plains. J. Biogeogr. 21 (3), 321.
Fyfe, R.M., Twiddle, C., Sugita, S., Gaillard, M., Barratt, P., Caseldine, C.J., Dodson, J., Edwards, K.J., Farrell, M., Froyd, C., Grant, M.J., Huckerby, E., Innes, J.B., Shaw, H., Waller, M., 2013. The Holocene vegetation cover of Britain and Ireland: overcoming

problems of scale and discerning patterns of openness. Quat. Sci. Rev. 73, 132-148.

Gallego-Sala, A.V., Charman, D.J., Brewer, S., Page, S.E., Prentice, I.C., Friedlingstein, P., Moreton, S., Amesbury, M.J., Beilman, D.W., Björck, S., Blyakharchuk, T., Bochicchio, C., Booth, R.K., Bunbury, J., Camill, P., Carless, D., Chimner, R.A., Clifford, M., Cressey, E., Courtney-Mustaphi, C., De Vleeschouwer, F., de Jong, R., Fialkiewicz-Koziel, B., Finkelstein, S.A., Garneau, M., Githumbi, E., Hribjlan, J., Holmquist, J., Hughes, P.D.M., Jones, C., Jones, M.C., Karofeld, E., Klein, E.S., Kokfelt, U., Korhola, A., Lacourse, T., Le Roux, G., Lamentowicz, M., Large, D., Lavoie, M., Loisel, J., Mackay, H., MacDonald, G.M., Makila, M., Magnan, G., Marchant, R., Marcisz, K., Martínez Cortizas, A., Massa, C., Mathijssen, P., Mauquoy, D., Mighall, T., Mitchell, F.J.G., Moss, P., Nichols, J., Oksanen, P.O., Orme, L., Packalen, M.S., Robinson, S., Roland, T.P., Sanderson, N.K., Sannel, A.B.K., Silva-Sánchez, N., Steinberg, N., Swindles, G.T., Turner, T.E., Uglow, J., Väliranta, M., van Bellen, S., van der Linden, M., van Geel, B., Wang, G., Yu, Z., Zaragoza-Castells, J., Zhao, Y., 2018. Latitudinal limits to the predicted increase of the peatland carbon sink with warming. Nat. Clim. Change. 8, 907-913.

Gao, G.Z., 2019. Records of topsoil phytopherites of typical plant communities in Northeast China and quantitative reconstruction of paleo-vegetation since Late Glacial Age. Northeast Normal University. 119-126.

Gao, G.Z., Evett, R., Li, N.N., Li, D.H., Wang, J.Y., Niu, H.H., Meng, M., Liu, Y., Jie, D.M., 2022. East Asian monsoon modulated Holocene spatial and temporal migration of forest-grassland ecotone in Northeast China. Catena 213, 106151.

Gao, G.Z., Li, D.H., Jie, D.M., Li, N.N, Liu, L.D., Liu, H.Y., Wang, J.Y., Niu, H.H., Meng, M., Liu, Y., Zhang, G.H., 2021. Application of soil phytoliths to the quantitative characterization of temperate grassland ecosystems: a case study in Northeast China. Plant Soil. 459 (1), 329-342.

Garnier, A., Neumann, K., Eichhorn, B., Lespez, L., 2013. Phytolith taphonomy in the middle- to late-Holocene fluvial sediments of Ounjougou (Mali, West Africa). The Holocene, 23(3), 416-431.

Guo, L.C., Xiong, S., Yang, P., Ye, W., Jin, G., Wu, W., Zhao, H., 2018. Holocene environmental changes in the Horqin desert revealed by OSL dating and δ13C analyses of paleosols. Quat. Int. 469, 11-19.

Hong, Y.T., Wang, Z.G., Jiang, H.B., Lin, Q.H., Hong, B., Zhu, Y.X., Wang, Y., Xu, L.S., Leng, X.T., Li, H.D., 2001. A 6000-year record of changes in drought and precipitation in northeastern China based on a δ13C time series from peat cellulose. Earth & Planetary Science Letters, 185, 111-119.

Hong, Y.T., Hong, B., Lin, Q.H., Shibata, Y., Hirota, M., Zhu, Y.X., Leng, X.T., Wang, Y., Wang, H., Yi, L., 2005. Inverse phase oscillations between the East Asian and Indian

Ocean summer monsoons during the last 12000 years and paleo-El Niño. Earth & Planetary Science Letters, 231(3-4), 337-346.

Hong, Y.T., Hong, B., Lin, Q.H., Shibata, Y., Zhu, Y.X., Leng, X.T., Wang, Y., 2009. Synchronous climate anomalies in the western North Pacific and North Atlantic regions during the last 14,000 years. Quaternary Science Reviews, 28 (9-10), 840-849.

Jie, D.M., Liu, Y.Y., 2012. Holocene environmental evolution in Northeast China (in Chinese). Northeast Normal University Press. 1-219.

Johnson, W.C., Millett, B.V., Gilmanov, T., Voldseth, R.A., Guntenspergen, G.R., Naugle, D.E., 2005. Vulnerability of Northern Prairie Wetlands to Climate Change. Bioscience. 55, 863-872.

Kang, S.G., Du, J.H., Wang, N., Dong, J.B., Wang, D., Wang, X.L., Qiang, X.K., Song, Y.G., 2020. Early Holocene weakening and mid-to late Holocene strengthening of the East Asian winter monsoon. Geology. 48 (11), 1043-1047.

Lacourse, T., Davies, M.A., 2015. A multi-proxy peat study of Holocene vegetation history, bog development, and carbon accumulation on northern Vancouver Island, Pacific coast of Canada. The Holocene 25, 1165-1178.

Li, J.D., Wu, B.H., Sheng, L.X., 2001. Jilin Vegetation. Jilin Science and Technology Press, Changchun (in Chinese).

Li, N.N., Chambers, F.M., Yang, J.X., Jie, D.M., Liu, L.D., Liu, H.Y., Gao, G.Z., Gao, Z., Li, D.H., Shi, J.C., Feng, Y.Y., Qiao, Z.H., 2017. Records of East Asian monsoon activities in Northeastern China since 15.6 ka, based on grain size analysis of peaty sediments in the Changbai Mountains. Quat. Int. 447, 158-169.

Liu, Z., Ma, X., Yang, F., Diao, H., Li, Y., 2024. Organic carbon storage and accumulation characteristics of peatlands in the Changbai Mountains, China. Land Degradation & Development, 35(1), 224-237.

Loisel, J., Gallego-Sala, A.V., Amesbury, M.J., Magnan, G., Anshari, G., Beilman, D.W., Benavides, J.C., Blewett, J., Camill, P., Charman, D.J., Chawchai, S., Hedgpeth, A., Kleinen, T., Korhola, A., Large, D., Mansilla, C.A., Müller, J., van Bellen, S., West, J.B., Yu, Z., Bubier, J.L., Garneau, M., Moore, T., Sannel, A.B.K., Page, S., Väliranta, M., Bechtold, M., Brovkin, V., Cole, L.E.S., Chanton, J.P., Christensen, T.R., Davies, M.A., De Vleeschouwer, F., Finkelstein, S.A., Frolking, S., Gałka, M., Gandois, L., Girkin, N., Harris, L.I., Heinemeyer, A., Hoyt, A.M., Jones, M.C., Joos, F., Juutinen, S., Kaiser, K., Lacourse, T., Lamentowicz, M., Larmola, T., Leifeld, J., Lohila, A., Milner, A.M., Minkkinen, K., Moss, P., Naafs, B.D.A., Nichols, J., O'Donnell, J., Payne, R., Philben, M., Piilo, S., Quillet, A., Ratnayake, A.S., Roland, T.P., Sjögersten, S., Sonnentag, O., Swindles, G.T., Swinnen, W., Talbot, J., Treat, C., Valach, A.C., Wu, J., 2021. Expert assessment of future vulnerability of the global peatland carbon sink. Nat. Clim. Chang. 11, 70-77.

Loisel, J., van Bellen, S., Pelletier, L., Talbot, J., Hugelius, G., Karran, D., Yu, Z.C., Nichols, J., Holmquist, J., 2017. Insights and issues with estimating northern peatland carbon stocks and fluxes since the last glacial maximum. Earth-Sci. Rev. 165, 59-80.

Lou, Y.J., Wang, G.P., Lu, X.G., Jiang, M., Zhao, K.Y., 2013. Zonation of plant cover and environmental factors in wetlands of the Sanjiang Plain, northeast China. Nord. J. Bot. 31, 748-756.

Lu, Y., Fang, X.M., Friedrich, O., Song, C.H., 2018. Characteristic grain-size component - A useful process-related parameter for grain-size analysis of lacustrine clastics? Quat. Int. 479, 90-99.

Mathijssen, P.J.H., Gałka, M., Borken, W., Knorr, K.H., 2019. Plant communities control long term carbon accumulation and biogeo-chemical gradients in a patagonian bog. Sci. Total. Environ. 684, 670-681.

Mathijssen, P.J.H., Väliranta, M., Korrensalo, A., Alekseychik, P., Vesala, T., Rinne, J., Tuittila, E.S., 2016. Reconstruction of Holocene carbon dynamics in a large boreal peatland complex, southern Finland. Quat. Sci. Rev. 142, 1-15.

Mazier, F., Broström, A., Bragée, P., Fredh, D., Stenberg, L., Thiere, G., Sugita, S., Hammarlund, D., 2015. Two hundred years of land-use change in the South Swedish Uplands: comparison of historical map-based estimates with a pollen-based reconstruction using the landscape reconstruction algorithm. Veg. Hist. Archaeobot. 24 (5), 555-570.

McLaren, P., Bowles, D., 1985. The effects of sediment transport on grain-size distributions. J. Sediment. Res. 55 (4), 457-470.

Neumann, K., Fahmy, A.G., Müller-Scheeßel, N., Schmidt, M., 2017. Taxonomic, ecological and palaeoecological significance of leaf phytoliths in West African grasses. Quat. Int. 434, 15-32.

Neumann, K., Strömberg, C.A.E., Ball, T., Albert, R.M., Vrydaghs, L., Cummings, L.S., 2019. International Code for Phytolith Nomenclature (ICPN) 2.0. Ann. Bot.-London 124, 189-199.

Niu, H.H., Sun, Y.H., Wang, J.Y., Marquer, L., Vessies, J., Sack, D., Chambers, F., Jie, D.M., 2024. Drivers of land cover and plant compositional changes in Northeast China since the mid-Holocene: Climate versus human activities. J. Archaeol. Sci. 163, 105938.

Niu, Z.G., Zhang, H.Y., Wang, X.W., Yao, W.B., Zhou, D.M., Zhao, K.Y., Zhao, H., Li, N.N., Huang, H.B., Li, C.C., Yang, J., Liu, C.X., Liu, S., Wang, L., Li, Z., Yang, Z.Z., Qiao, F., Zheng, Y.M., Chen, Y.L., Sheng, Y.W., Gao, X.H., Zhu, W.H., Wang, W.Q., Wang, H., Weng, Y.L., Zhuang, D.F., Liu, J.Y., Luo, Z.C., Cheng, X., Guo, Z.Q., Gong, P., 2012. Mapping wetland changes in China between 1978 and 2008. Chin. Sci. Bull. 57, 2813-2823.

Panait, A., Diaconu, A., Galka, M., Grindean, R., Hutchinson, S.M., Hickler, T., Lamentowicz, M., Mulch, A., Tanţău, I., Werner, C., Feurdean, A., 2017. Hydrological conditions and carbon accumulation rates reconstructed from a mountain raised bog in the carpathians: A multi-proxy approach. Catena 152, 57-68.

Panait, A., Diaconu, A., Galka, M., Grindean, R., Hutchinson, S.M., Hickler, T., Lamentowicz, M., Mulch, A., Tanţău, I., Werner, C., Feurdean, A., 2017. Hydrological conditions and carbon accumulation rates reconstructed from a mountain raised bog in the carpathians: A multi-proxy approach. Catena 152, 57-68.

Piotrowska, N., Blaauw, M., Mauquoy, D., Chambers, F.M., 2011. Constructing deposition chronologies for peat deposits using radiocarbon dating. Mires Peat. 7 (10), 1-14.

Piperno, D.R., 2006. Phytoliths: A Comprehensive Guide for Archaeologists and Paleoecologists. AltaMira Press, Lanham, MD, p. 238.

Qu, X.X., Huang, C., Rao, Z.G., Wei, G.J., Wu, L.Y., Luo, Y.Y., Li, Y.X., Zhao, L., Liu, L.D., Deng, W.F., 2024. Holocene provenance variations and palaeofloods response to ENSO-driven monsoon precipitation in the subalpine peatland in southern China. Palaeogeogr. Palaeoclimatol. Palaeoecol. 635, 111948.

Stebich, M., Rehfeld, K., Schlutz, F., Tarasov, P.E., Liu, J.Q., Mingram, J., 2015. Holocene vegetation and climate dynamics of NE China based on the pollen record from Sihailongwan Maar Lake. Quat. Sci. Rev. 124, 275-289.

Strömberg, C.A.E., 2004. Using phytolith assemblages to reconstruct the origin and spread of grass-dominated habitats in the great plains of North America during the late Eocene to early Miocene. Palaeogeogr. Palaeoclimatol. Palaeocol. 207, 239-275.

Strömberg, C.A.E., Werdelin, L., Friis, E.M., Sarac, G., 2007. The spread of grassdominated habitats in Turkey and surrounding areas during the Cenozoic: phytolith evidence. Palaeogeogr. Palaeoclimatol. Palaeoecol. 250, 18-49.

Sun, J.J., Li, H.C., Wang, J., Zhao, H.Y., Wang, S.Z., Li, H.K., Yang, Q.N., Chou, C.Y., Kashyap, S., 2019. Study of Jinchuan Mire in NE China II: Peatland development, carbon accumulation and climate change during the past 1000 years. Quat. Int. 528, 18-29.

Sun, X.H., Zhao, Y., Li, Q.,2017. Holocene peatland development and vegetation changes in the Zoige Basin, eastern Tibetan Plateau. Sci. China. Earth. Sci. 60, 1826-1837.

Swinnen, W., Broothaerts, N., Verstraeten, G., 2021. Modelling long-term alluvial-peatland dynamics in temperate river floodplains, Biogeosciences, 18, 6181-6212.

Twiss, P. C., 1992. Predicted World Distribution of C3 and C4 Grass Phytoliths. New York: Plenum Press. 113-128.

van Bellen, S., Dallaire, P.L., Garneau, M., Bergeron, Y., 2011. Quantifying spatial and temporal Holocene carbon accumulation in ombro-trophic peatlands of the Eastmain region, Quebec, Canada. Glob. Biogeochem. Cycle. 25, GB2016.

Vandenberghe, J., Sun, Y.B., Wang, X.Y., Abels, H.A., Liu, X.X., 2018. Grain-size characterization of reworked fine-grained aeolian deposits. Earth Sci. Rev. 177, 43-52.

Visher, G.S., 1969. Grain size distributions and depositional processes. J. Sediment. Res. 39 (3), 1074-1106.

Wang, C.L., Zhao, H.Y., Wang, G.P., 2015a. Vegetation development and water level changes in Shenjiadian Peatland in Sanjiang Plain, Northeast China. Chin. Geogr. Sci. 25 (4), 451-461.

Wang, M., Chen, H., Wu, N., Peng, C.H., Zhu, Q.A., Zhu, D., Yang, G., Wu, J.H., He, Y.X., Gao, Y.H., Tian, J.Q., Zhao, X.Q., 2014. Carbon dynamics of peatlands in China during the Holocene. Quat. Sci. Rev. 99, 34-41.

Wang, M., Yang, G., Gao, Y.H., Chen, H., Wu, N., Peng, C.H., Zhu, D., Wu, J.H., He, Y.X., Tian, J.Q., Zhao, X.Q., Zhang, Y., 2015. Higher recent peat C accumulation than that during the Holocene on the Zoige Plateau. Quat. Sci. Rev. 114, 116-125.

Wang, Y.C., Han, Z.Y., Zhou, Y.W., Chen, J., Li, X.S., Wang, Y., Yi, S.W., Lu, H.Y., 2022. A quantitative reconstruction of Holocene annual precipitation in the marginal zone of the East asian summer monsoon. Palaeogeogr. Palaeoclimatol. Palaeoecol. 596, 110968.

Wu, J., Shen, J., 2010. Paleoenvironmental and Paleoclimatic changes in Lake Xingkai inferred from stable carbon and nitrogen isotopes of bulk organic matter since 28 ka BP. Acta Sedentol. Sin. 28 (2), 365-372 (in Chinese with English abstract).

Xia, Y.M., Wang, P.F., 2000. Peat record of climate change since 3000 years, in Yangmu, Mishan region (in Chinese). Geogr. Res-aust. 01, 53-59.

Xia, Y.Y., Li, H.C., Zhao, H.Y., Wang, S.Z., Li, H.K., Yan, H., 2019. Peatland development and environmental change during the past 1600 years in Baijianghe Mire of Changbai Mountains, China. Quat. Int. 528, 41-52.

Xing, W., Bao, K., Guo, W., Lu, X., Wang, G., 2015. Peatland initiation and carbon dynamics in Northeast China: Links to holocene climate variability. Boreas. 44, 575-587.

Xu, D.K., Lu, H.Y., Chu, G.Q., Liu, L., Shen, C.M., Li, F.J., Wang, C., Wu, N.Q., 2019. Synchronous 500-year oscillations of monsoon climate and human activity in Northeast Asia. Nat. Commun. 10 (1), 1-10.

Yang, Z., Gao, G.Z., Jie, D.M., Wang, J.Y., Niu, H.H., Liu, Z.P., Meng, M., Song, L.N., Chen, N.K., Wei, Y.X., Yu, J.H., 2023. Holocene vegetation dynamics of Horqin Sandy Land in northern China inferred from the phytolith record of a sand-paleosol section. Palaeogeogr. Palaeoclimatol. Palaeoecol. 622, 11571.

Yu, Z.C., 2011. Holocene carbon flux histories of the world’s peatlands. Holocene. 21, 761-774.

Yu, Z.C., Joos, F., Bauska, T.K., Stocker, B.D., Fischer, H., Loisel, J., Brovkin, V., Hugelius, G., Nehrbass-Ahles, C., Kleinen, T., Schmitt, J., 2021. No support for carbon storage of >1,000 GtC in northern peatlands. Nat. Geosci. 14, 465-467.

Zhang, M.M., Bu, Z.J., Jiang, M., Wang, S.Z., Liu, S.S., Jin, Q., Shi, P.H., 2019. Mid-late

Holocene maar lake-mire transition in northeast China triggered by hydroclimatic variability. Quat. Sci. Rev. 220, 215-229.

Zhang, M.M., Bu, Z.J., Liu, S.S. Chen, J., Cui, Y.X., Chen, X., 2020. Lake-mire ecosystem transformation and its possible forcing mechanisms in volcanic landform regions: a case study in the Gushantun peatland of northeast China. Earth Surf. Process. Landforms 45, 3141-3154.

Zhang, M.M., Bu, Z.J., Liu, S.S., Chen, J., Cui, Y.X., 2021. Mid-late Holocene peatland vegetation and hydrological variations in Northeast Asia and their responses to solar and ENSO activity. Catena 203, 105339.

Zhang, Y., Yang, P. , Gao, C.Y., Tong, C., Zhang, X.Y., Liu, X.T., Zhang, S.Q., A. Meyers, p., 2020. Peat properties and Holocene carbon and nitrogen accumulation rates in a peatland in the Xinjiang Altai Mountains, northwestern China. J. Geophys. Res-biogeo. 125, e2019JG005615.

Zhang, Z., Xing, W., Lu, X., Wang, G., 2014. The grain-size depositional process in wetlands of the Sanjiang Plain and its links with the East Asian monsoon var-iations during the Holocene. Quat. Int. 349, 245-251.

Zhang, Z.Q., Xing, W., Wang, G.P., Tong, S.Z., Lv, X.G., Sun, J.M., 2015. The peatlands developing history in the Sanjiang Plain, NE China and its response to East Asian monsoon variation. Sci. Rep. 5, 11316.

Zhao, H.Y., Leng, X.T., Wang, S.Z., 2002. Distribution Accumulation Rate of Peat in the Changbaishan Mountains and Climate Change in Holocene (in Chinese). J. Mt. Sci. 05, 513-518.

Zhao, J., Tan, L., Yang, Y., Pérez-Mejías, C., Brahim, Y.A., Lan, J., Wang, J., Li, H., Wang, T., Zhang, H., Cheng, H., 2021. New insights towards an integrated understanding of NE Asian monsoon during mid to late Holocene. Quat. Sci. Rev. 254, 106793.

Zhao, M., Wang, M., Zhao, Y., Hu, N., Wang, G., Jiang, M., 2023. Variations in microbial carbon metabolic activities in sedge peatlands along an altitudinal gradient in the Changbai Mountain, China. Catena 220, 106722.

Zhao, Y., Tang, Y., Yu, Z.C., Li, H., Yang, B., Zhao, W.W., Li, F.R., Li, Q., 2014. Holocene peatland initiation, lateral expansion, and carbon dynamics in the Zoige Basin of the eastern Tibetan Plateau. The Holocene 24(9), 1137-1145.

Zhao, Y., Yu, Z., 2012. Vegetation response to Holocene climate change in East Asian monsoon-margin region. Earth Sci. Rev. 113, 1-10.

Zheng, Y.H., Pancost, R.D., Liu, X.D., Wang, Z.Z., Naafs, B., Xie, X.X., Liu, Z., Yu, X.F., Yang, H., 2017. Atmospheric connections with the North Atlantic enhanced the deglacial warming in northeast China. Geology, 45 (11), 1031-1034.